

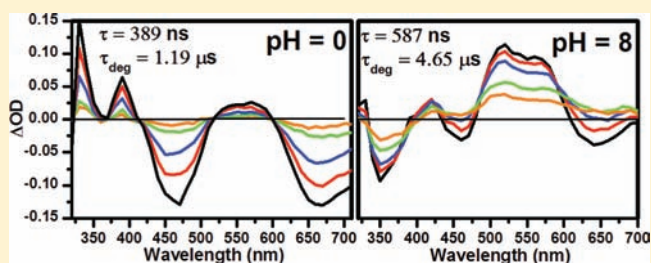
pH Control of Intramolecular Energy Transfer and Oxygen Quenching in Ru(II) Complexes Having Coupled Electronic Excited States

Tod A. Grusenmeyer,[†] Jin Chen,[†] Yuhuan Jin,[‡] Jonathan Nguyen,[†] Jeffrey J. Rack,[‡] and Russell H. Schmehl^{*,†}

[†]Department of Chemistry, Tulane University, New Orleans, Louisiana 70118, United States

[‡]Department of Chemistry and Biochemistry, Ohio University, Athens, Ohio 45701, United States

ABSTRACT: This work illustrates the control of excited state energy transfer processes via variation of pH in transition metal complexes. In these systems a Ru(II) complex having two carboxylated bipyridyl ligands is covalently linked to pyrene via one of two different pyrene derivitized bipyridyl ligands. The energy of the Ru to carboxy-bipyridine ³MLCT state is pH dependent while the pyrene triplet energy remains unchanged with solution acidity. At pH 0 the ³MLCT state is the lowest energy state, and as the pH is raised and the carboxy-bipyridyl ligands are successively deprotonated, the energy of the ³MLCT state rises above that of the pyrene triplet, resulting in a significant increase in the lifetime of the observed emission. Detailed analysis of ultrafast and microsecond time-resolved excited state decays result in a description of excited state decay that involves initial equilibration of the ³MLCT and pyrene triplet states followed by relaxation to the ground state. The lifetime of excited state decay is defined by the position of the equilibrium, going from 2 μs at pH 0 to >10 μs at higher pH as the equilibrium favors the pyrene triplet. In addition, quenching of the excited state by dissolved oxygen exhibits a pH dependence that parallels that of the excited state lifetime. The results illustrate the utility of exploiting excited state equilibria of this type in the development of highly effective luminescent oxygen sensors.



INTRODUCTION

The dissipation of excitation energy can be quite complex in electronically excited chemical systems that contain two or more independent (or weakly coupled) chromophores with excited state energies separated by relatively small energy gaps.^{1–3} The excitation energy can be shuttled between the independent chromophores while the system as a whole relaxes to the ground state.⁴ If one of the chromophoric units is photoreactive, additional relaxation paths are introduced. Recently there have been numerous reports of the photo-physical behavior of metal diimine complexes, mostly Ru(II), covalently linked to aromatic hydrocarbons.^{5–14} Figure 1 shows a generic state diagram for such complexes. Metal-to-ligand charge transfer (MLCT) excitation results in population of the triplet excited state manifold within a few hundred femtoseconds,¹⁵ with full thermal equilibration on the picosecond time scale.^{16,17} The triplet MLCT state formed initially can, depending on the energy gap and nature of the covalent linkage, transfer energy reversibly to the pendant aromatic hydrocarbon chromophore (³IL). There has been considerable attention given to this topic because of the reversible energy transfer between the ³MLCT state and the ³IL state of pyrene, which has been summarized in reviews.^{12,18} For many of these systems, the triplet MLCT state is luminescent, and the observed effect of this reversible energy transfer is an increase

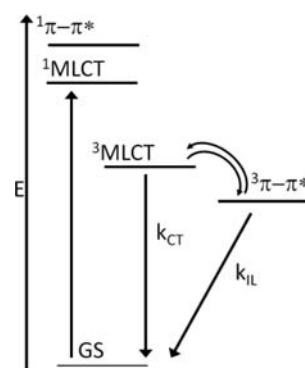


Figure 1. Generalized state diagram for complexes having nearly isoenergetic MLCT and IL excited states.

in the lifetime of the luminescence, ascribed to the long lifetimes of the ³IL states.^{5,19,20} In addition, the luminescence generally exhibits a greater sensitivity to oxygen quenching which is directly related to the longer lived covalently linked aromatic hydrocarbon triplet state.²¹ Recently such covalently linked bichromophoric molecules have been used as sensitive

Received: January 26, 2012

Published: March 31, 2012

phosphorescent indicators of dissolved oxygen in hypoxic environments.²¹ The key to observing the reversible energy transfer in these systems is maintaining a small ($<1000\text{ cm}^{-1}$; $<3\text{ kcal}$) energy gap between the participating excited states, although details of the free energy dependence of the reversible energy transfer and the overall relaxation are lacking.

In the late 1970s, Wrighton and co-workers reported the photophysical behavior of Ru(II) complexes having a single 4,4'-dicarboxy-2,2'-bipyridine (dcbH₂) ligand.²² In aqueous solution the luminescence energy of the complex decreases upon decreasing the pH of the solution and protonation of the carboxyl groups of the substituted bipyridine. The authors also demonstrated that the average pK_a of the carboxyl ligands is greater when the complex is in the ³MLCT state, consistent with an increase in electron density on the carboxy-bipyridine ligand in the excited state. More recently Nazeeruddin et al. thoroughly examined the ground and excited state acid dissociation processes of [(bpy)Ru(dcbH₂)₂]Cl₂ in solutions of sulfuric acid and sodium hydroxide.²³ While there are four dissociable protons in the complex, only two experimentally distinct pK values were determined, indicating that the first deprotonation from each bpy occurs at or near the same pH. Moreover, the authors demonstrated that, just as with [(bpy)₂Ru(dcbH₂)₂]Cl₂, the luminescence maximum was dependent on pH over the pH range 0–7. These data show that the energy of the luminescent excited state can be controlled with pH.

In this manuscript, the use of pH to control the ³MLCT state energy is exploited in examination of reversible energy transfer between the ³MLCT state and the ³IL state of a covalently attached aromatic hydrocarbon. The systems examined involve Ru(II) complexes having carboxylated diimine ligands and one of two covalently linked bipyridyl pyrene ligands. The rate of the energy transfer process and the position of equilibrium can be systematically controlled by varying the pH of the medium. Through a combination of ultrafast and nanosecond time-resolved transient absorption experiments, the dynamics of the intramolecular energy transfer and the relaxation of the equilibrated excited state are clearly elucidated. The importance of pH on excited state reactivity is clearly illustrated in the oxygen quenching sensitivity. These systems are under investigation as *in vivo* phosphorescent sensors for dissolved oxygen. This work illustrates the strong dependence of the oxygen sensing ability to small differences in energy gap between the emitting ³MLCT state and the ³IL state of the pyrene. As shown here, it is the excited state lifetime and not differences in the quenching rate constant between the ³MLCT and ³IL states that leads to the pH sensitivity of oxygen quenching.

EXPERIMENTAL SECTION

Spectroscopy. NMR spectra were recorded on a Varian 400 MHz NMR. ESI mass spectra were obtained using a Bruker microTOF spectrometer. All UV–vis absorption spectra were obtained on a Hewlett-Packard 8452A diode array spectrophotometer. Photoluminescence spectra were obtained using a Spex Fluorolog Fluorimeter equipped with a 450 W Xe arc lamp and a SPEX 0.34 m spectrograph/CCD detector (Andor IDUS). Photoluminescence lifetime measurements were collected using the visible output of an OPO (OPOTEK) which was pumped by the third harmonic of a Quantel Brilliant B Q-switched Nd:YAG laser. Excitation pulses were generally $<5\text{ ns}$ and were tuned to the absorption λ_{max} of each chromophore. Emitted light was detected through a single grating monochromator (Applied Photophysics 0.25 m) with PMT detection

(Hamamatsu R928). The output was recorded on an Agilent Infinium transient digitizer. Each decay was recorded at the emission λ_{max} and was the average of 5000 pulses.

Nanosecond Time-Resolved Transient Absorption. Nanosecond transient absorption measurements were performed using a Quantel Brilliant B Q-switched Nd:YAG laser-pumped OPO (Opotek) as the pump source at a right angle to the analyzing light source. Excitation pulses were $<5\text{ ns}$ and were tuned to the λ_{max} of the compound being interrogated. An Applied Photophysics LKS.60 laser flash photolysis spectrometer was used for detection; the instrument is equipped with a 150 W pulsed Xe arc lamp as the analyzing light source, a single grating monochromator (Applied Photophysics 0.25 m) after the sample, and PMT detection (Hamamatsu R928). The output was recorded on an Agilent Infinium transient digitizer and decays and spectra were acquired and analyzed with Applied Photophysics LKS.60 software.

Femtosecond Time-Resolved Transient Absorption. Femtosecond transient absorption measurements were collected on an Ultrafast Systems Helios transient absorption spectrometer. A Spectra Physics Solstice laser, a one-box regenerative amplifier containing a Mai Tai femtosecond oscillator and Empower pump laser, was employed to produce 800 nm pulses at a repetition rate of 1 kHz at 3.5 W average power and a pulse width of $<100\text{ fs}$. From this unit, the beam is split (50:50) with one beam directed to an optical parametric amplifier (TOPAS, Light Conversion) and the other to the Helios spectrometer (HE-vis-3200) to create the pump (472 nm; TOPAS) and probe (Helios) sources, respectively. The 800 nm probe beam passed through a CaF₂ plate to generate a white light continuum ($\sim 330\text{--}700\text{ nm}$). The spectrum was integrated for 2 s for each scan. The pump and probe beams were directed to a 2 mm path length cuvette containing the sample where they were spatially overlapped. The solution was vigorously stirred in the 2 mm path length cuvette during data collection. Transient absorption data were corrected by subtracting spectral background features that persisted from the previous pulse and appeared prepulse as well as applying chirp correction using Surface Explorer Pro 1.1.5 software (Ultrafast Systems).

Syntheses. The ligands and complexes 4-(1-pyrenyl)-2,2'-bipyridine (pyr-bpy),²⁴ 2,2'-bipyridine-4,4'-dicarboxylic acid (dcbH₂),²⁵ *cis*-[Ru(dcbH₂)Cl₂],²⁶ and [(Bz)Ru(bpy)Cl]Cl (Bz = benzene)²⁷ were all prepared as reported in a previous work.

4-(p-(1-Pyrenyl)phenyl)-2,2'-bipyridine (pyr-phen-bpy). A total of 0.48 g (1.45 mmol) of 4,4,5,5-tetramethyl-2-(1-pyrenyl)-1,3,2-dioxborolane and 0.45 g (1.45 mmol) of 4-(4-bromophenyl)-2,2'-bipyridine were dissolved in 25 mL of toluene. The mixture was purged with N₂ for 15 min. Fifteen ml of 1 M NaOH and 33.5 mg (2 mol %) Pd(PPh₃)₄ were then added to the mixture. The reaction was run under reflux for 20 h. After the reaction, the organic and aqueous phases were separated. The aqueous layer was extracted with toluene (4 × 20 mL). The organic phases were combined and dried with MgSO₄. The solvent was then removed via rotary evaporation. The residue was purified by column chromatography on silica gel using a gradient of 20:1–1:1 hexanes: ethyl acetate. After purification, 0.37 g (60% yield) of a light yellow solid was obtained. ¹HNMR (CDCl₃) δ ppm: 8.82 (ds, $J = 1.84\text{ Hz}, 0.73\text{ Hz}, 1\text{ H}$), 8.80 (dd, $J = 5.08\text{ Hz}, 0.75\text{ Hz}, 1\text{ H}$), 8.75 (ddd, $J = 4.77\text{ Hz}, 1.80\text{ Hz}, 0.92\text{ Hz}, 1\text{ H}$), 8.50 (td, $J = 8.00\text{ Hz}, 1.05\text{ Hz}, 1.05\text{ Hz}, 1\text{ H}$), 8.28–8.18 (m, 4H), 8.13 (s, 2H), 8.09–8.01 (m, 3H), 7.99 (td, $J = 8.4\text{ Hz}, 2\text{ H}$), 7.88 (dt, $J = 8\text{ Hz}, 1.8\text{ Hz}, 1\text{ H}$), 7.79 (td, $J = 8.4\text{ Hz}, 2\text{ H}, 2\text{ H}$), 7.68 (dd, $J = 5.08\text{ Hz}, 1.88\text{ Hz}, 1\text{ H}$), 7.36 (ddd, $J = 7.50\text{ Hz}, 4.76\text{ Hz}, 1.19\text{ Hz}, 1\text{ H}$). ¹³CNMR (CDCl₃) δ ppm: 156.53, 155.87, 149.60, 149.24, 142.24, 137.18, 137.03, 136.83, 132.27, 132.23, 132.10, 131.53(2), 131.36, 131.01, 130.88, 128.76, 128.64, 128.54, 128.48, 127.80, 127.69, 127.54, 127.25 (2), 126.16, 125.04, 124.93, 127.78, 121.65, 121.49, 119.22. ESI-MS (m/z): 433.1762 [M+H]⁺ (Calcd. 433.1699, 14.54 ppm).

[(dcbH₂)₂Ru(bpy)]Cl₂. A total of 75 mg of [(Bz)Ru(bpy)Cl]Cl and 95.1 mg of dcbH₂ were added to 2 mL of DMF. The mixture was refluxed under nitrogen for 4 h during which the reaction color changed from yellow to purple to dark red. After the reaction, the mixture was added to 50 mL of acetone and cooled in the freezer to

precipitate the product. A total of 100.2 mg (72.6%) of dark red solid was collected on the fritted glass. Of this solid 25 mg was purified via prep TLC. The compound was eluted with a 1:1 mixture of 0.25 M HCl:CH₃CN on 1 mm thick silica. Three distinct bands are observed on the silica plate. A yellow band with an *R_f* value of approximately 0.80 and a purple band with an *R_f* value of approximately 0.75 completely separate from a fluorescent orange band that streaks over the bottom third of the TLC plate. The fluorescent orange material was collected by rinsing the silica with water. A total of 16.2 mg (64.8%) of orange solid was obtained after the water was removed via rotary evaporation. ¹HNMR (CD₃OD with one drop of NaOH in D₂O) δ ppm: 9.05 (s, 4H), 8.69 (d, *J* = 8.1 Hz, 2H), 8.12 (t, *J* = 7.8 Hz, 2H), 7.88 (d, *J* = 5.7 Hz, 2H), 7.82 (m, 8H), 7.49 (t, *J* = 6.5 Hz, 2H).

[(dcbH₂)₂Ru(pyr-bpy)]Cl₂. A total of 125 mg (0.18 mmol) of *cis*-[(dcbH₂)₂Ru(bpy)]Cl₂ was dissolved in 5 mL of 0.1 M NaOH and 10 mL of EtOH. A 5 mL solution of 86 mg of (0.2 mmol) pyr-bpy in CHCl₃ was then added to the mixture. The reaction was refluxed for 17 h. Upon completion of the reaction, the solvent was removed via rotary evaporation until approximately 5 mL remained. 0.1 M NaOH was added dropwise to the solution until the pH 8. The mixture was then filtered. The filtrate was collected and acidified with 0.2 M HCl until pH 2.7 and centrifuged. The solid was isolated and excess ligand impurity was removed via Soxhlet extraction with CH₂Cl₂ until no blue fluorescence was observed when irradiated with a UV hand lamp. After extraction, 115 mg of dark red solid was obtained (62% yield). ¹HNMR (CD₃OH with one drop of NaOH in D₂O) δ ppm: 9.19 (1H, s), 9.14–9.16 (3H, m), 9.02 (1H, s), 8.82 (1H, d, *J* = 7.9 Hz), 8.36 (1H, d, *J* = 7.9 Hz), 8.30 (1H, d, *J* = 8 Hz), 8.27 (1H, d, *J* = 7.9 Hz), 8.21–8.18 (5H, m), 8.16–8.12 (2H, m), 8.09 (1H, m), 8.06–8.01 (3H, m), 7.99 (2H, m), 7.94–7.91 (3H, m), 7.86 (1H, d, *J* = 6.2 Hz), 7.796 (1H, dd, *J* = 6 Hz, 1.8 Hz), 7.52 (1H, t, *J* = 7.2 Hz). ESI-MS: *m/z* = 517.0375 [M-4H+4Na]²⁺ (Calcd. 517.0303; 13.93 ppm difference), *m/z* = 471.0502 [M-4H]²⁺ (Calcd. 471.0507; 1.06 ppm difference), *m/z* = 449.0569 [M-4H-CO₂]²⁺ (Calcd. 449.0558; 2.45 ppm difference), *m/z* = 427.0616 [M-4H-2CO₂]²⁺ (Calcd. 427.0609; 1.64 ppm difference), *m/z* = 405.0666 [M-4H-3CO₂]²⁺ (Calcd. 405.0659; 1.73 ppm difference).

[(dcbH₂)₂Ru(pyr-phen-bpy)]Cl₂. The complex was synthesized using the same procedure as described above for [(dcbH₂)₂Ru(pyr-bpy)]Cl₂ but the pyr-phen-bpy ligand was substituted for pyr-bpy. A total of 125 mg (0.18 mmol) of *cis*-[Ru(dcbH₂)₂Cl₂] and 86 mg (0.20 mmol) of pyr-phen-bpy were used in the reaction, yielding 147 mg of a dark red solid (75% yield). ¹HNMR (CD₃OH with one drop of NaOH in D₂O) δ ppm: 9.07–9.03 (4H, m), 9.01 (1H, s), 8.90 (1H, d, *J* = 8.4 Hz), 8.29 (1H, d, *J* = 8 Hz), 8.26–8.20 (2H, m), 8.17–8.12 (5H, m), 8.11–8.04 (1H, m), 8.03 (1H, m), 7.98 (1H, d, *J* = 6 Hz), 7.93–7.87 (4H, m), 7.87–7.80 (10H, m), 7.50 (1H, t, *J* = 6 Hz). ESI-MS: *m/z* = 555.0547 [M-4H+4Na]²⁺ (Calcd. 555.0460; 15.67 ppm difference), *m/z* = 509.0637 [M-4H]²⁺ (Calcd. 509.0665; 5.50 ppm difference), *m/z* = 487.0684 [M-4H-CO₂]²⁺ (Calcd. 487.0715; 6.36 ppm difference), *m/z* = 465.0739 [M-4H-2CO₂]²⁺ (Calcd. 465.0766; 5.81 ppm difference).

RESULTS

Three heteroleptic ruthenium diimine complexes, [Ru(dcbH₂)₂(pyr-bpy)]Cl₂, [Ru(dcbH₂)₂(pyr-phen-bpy)]Cl₂, and [Ru(dcbH₂)₂(bpy)]Cl₂ where dcbH₂ is (4,4'-dicarboxy-2,2'-bipyridine, pyr-bpy is 4-(1-pyrenyl)-2,2'-bipyridine and pyr-phen-bpy is 4-(*p*-(1-pyrenyl)phenyl)-2,2'-bipyridine, were prepared and investigated. The pyrene containing complexes are depicted in Figure 2. The synthesis of the pyr-bpy ligand was reported earlier⁵ and the synthesis of the pyr-phen-bpy was achieved by Suzuki coupling of 4-(*p*-bromophenyl)-2,2'-bipyridine with pyrene-1-boronic acid; the boronic acid derivative was prepared from reaction of triisopropylborate with pyrene-1-bromide.²⁸ The complexes containing the pyrene modified bipyridine ligands were made by reaction of *cis*-

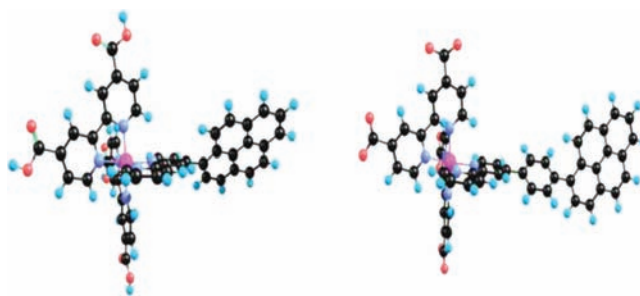


Figure 2. Graphical representations of the chromophores: [Ru(dcbH₂)₂(pyr-bpy)]²⁺ (left) and [Ru(dcbH₂)₂(pyr-ph-bpy)]²⁺ (right).

[(dcbH₂)₂RuCl₂] with the pyrene containing ligand. The complexes were characterized by ¹H NMR spectroscopy, ESI mass spectrometry in negative ion mode, UV–visible absorption spectroscopy, and cyclic voltammetry. A few of the complexes contain trace amounts (not detectable by ESI mass spectrometry) of a luminescent component, possibly [(dcbH₂)₂Ru] (vide infra) present in the reactant [(dcbH₂)₂RuCl₂].

Absorption and Luminescence Behavior. In basic water/methanol (1:1) solutions [Ru(dcbH₂)₂(bpy)]Cl₂ has two ligand localized absorption maxima, at 288 and 300 nm, as well as a single metal-to-ligand-charge transfer (MLCT) absorption at 462 nm with a shoulder at 436 nm. In acidic aqueous methanol solution, an interligand absorption is observed at 288 nm, but the ligand localized absorption at 300 nm shifts to 308 nm. Similarly, the metal-to-ligand charge transfer absorption is observed at 478 nm with a shoulder at 442 nm. No clear separation of the Ru to bpy MLCT and the Ru to dcbH₂ MLCT absorption bands is observed, regardless of the degree of protonation of the carboxylated bipyridine ligand. These results mirror those of Nazeruddin's earlier work.²³ The spectrophotometric characteristics of the pyrene-bipyridine containing chromophores have the same signatures as [Ru(dcbH₂)₂(bpy)]Cl₂ but also have a single broad band with a maximum between 300 and 400 nm that corresponds to a pyrene localized $\pi \rightarrow \pi^*$ transition. A consistent change in the MLCT spectra of all of the complexes is observed in lowering the pH from 8 to 0; in each case the absorbance of the shoulder increases to be equivalent with that of the 478 nm maximum.

The pyr-bpy ligand alone has little absorbance to the red or 350 nm, but the possibility exists that, upon coordination to a divalent metal center, new transitions may arise that absorb at lower energy. As a result, we prepared the Zn(II) complex of pyr-bpy by addition of an excess of zinc sulfate to a solution of the pyr-bpy ligand in water/methanol (1:1). Coordination of Zn(II) to the ligand results in broadening of the pyrene localized $\pi \rightarrow \pi^*$ absorption, but the absorbance reaches zero by 430 nm.

For all of the chromophores, the luminescence maximum gradually shifts to the red as the pH increases from 0 to 2.5. However, a much larger blue shift of the emission maximum occurs as the pH is further increased to 8. Figure 3 shows emission maxima as a function of pH for [(dcbH_n)₂Ru(pyr-bpy)]⁽²ⁿ⁻²⁾ (*n* = 0–2) in 1:1 water/methanol solutions. The spectra are broad, lack vibronic structure, and appear to have a bandwidth that does not change significantly with pH. The emission spectra of the pyrene containing complexes are quite similar to [(dcbH₂)₂Ru(bpy)], suggesting that the emission arises from the ³MLCT state.

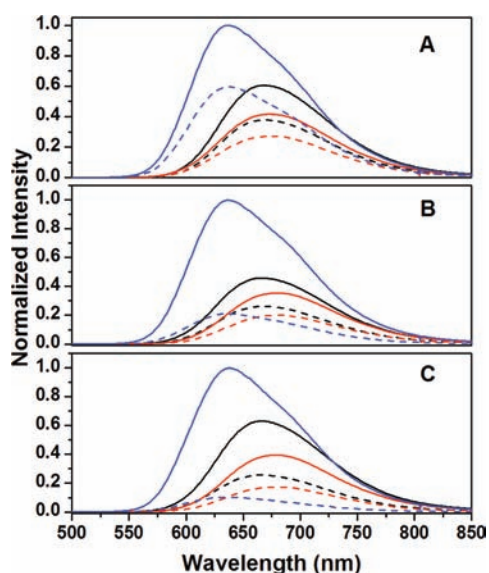


Figure 3. Oxygenated (---) and deoxygenated (—) luminescence spectra of the chromophores at pH 0 (black), pH 2.5 (red), and pH 8 (blue). (A) $[(\text{dcbH}_2)_2\text{Ru}(\text{bpy})]^{2+}$, (B) $[(\text{dcbH}_2)_2\text{Ru}(\text{pyr-ph-bpy})]^{2+}$, and (C) $[(\text{dcbH}_2)_2\text{Ru}(\text{pyr-bpy})]^{2+}$.

The sensitivity of the luminescence to oxygen quenching is also pH dependent, especially for the pyrene containing complexes, and is most sensitive in alkaline solution. Of the three complexes, the pyr-bpy chromophore exhibits the highest degree of oxygen quenching in air saturated solutions and the largest pH dependence. The quenching ratio (I_0/I) in basic aqueous methanol is 12.2, whereas the quenching ratio of the pyr-phen-bpy chromophore is 4.8, and the bpy complex luminescence is quenched only by a factor of 2. The luminescence spectra in oxygenated and deoxygenated solutions at three pH values are illustrated in Figure 3 for each of the chromophores. The oxygen quenching was also evaluated by changes in the luminescence lifetimes of the chromophores. The pyr-bpy complex has a lifetime quenching ratio in basic aqueous methanol of 27 and the pyr-phen-bpy chromophore has a quenching ratio of 7.5. The excited state lifetime pH dependence of the oxygen quenching is shown in Figure 4 for the two pyrene containing complexes. This figure clearly illustrates that, as the degree of protonation of the carboxybipyridine ligands increases (and the ${}^3\text{MLCT}$ state energy decreases), the degree of the oxygen quenching decreases.

Excited state lifetimes determined for $[\text{Ru}(\text{dcbH}_2)_2(\text{bpy})]\text{Cl}_2$ over the pH range 0 to 9 are single exponential and the degree of oxygen quenching is the same for both luminescence intensity and lifetime measurements. The behavior of the pyrene containing complexes is complicated by the fact that the decays become double exponential in neutral and basic solutions. Transient absorption decays, on the other hand, were cleanly single exponential at all pHs examined (vide infra). Since transient absorption is much less sensitive to impurity contributions than luminescence measurements, we believe that the additional luminescence decay component is due to traces of a complex impurity that lacks the pyrene modified bipyridine. The most likely impurity, based on the synthetic procedure employed is $[\text{Ru}(\text{dcbH}_2)_3]\text{Cl}_2$. The presence of luminescence from an impurity of this type would serve to explain the differences observed between intensity and lifetime

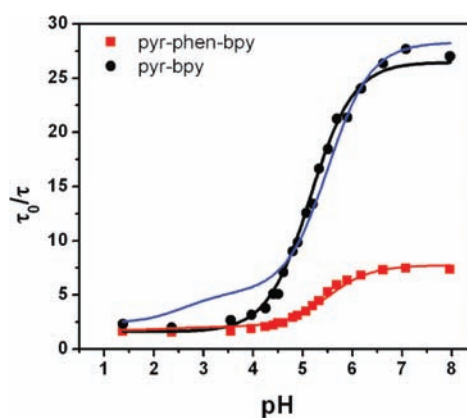


Figure 4. Ratio of the deoxygenated to oxygenated excited state lifetime for $[(\text{dcbH}_n)_2\text{Ru}(\text{pyr-bpy})]^{(2n-2)+}$ (●) and $[(\text{dcbH}_n)_2\text{Ru}(\text{pyrph-bpy})]^{(2n-2)+}$ (■) ($n = 0-2$) between pH 0 and 8. The black and red solid lines represent fits to the data using eq 9. The blue line represents the best fit obtained using a single quenching rate constant for the ${}^3\text{MLCT}$ and ${}^3\text{IL}$ states (see text).

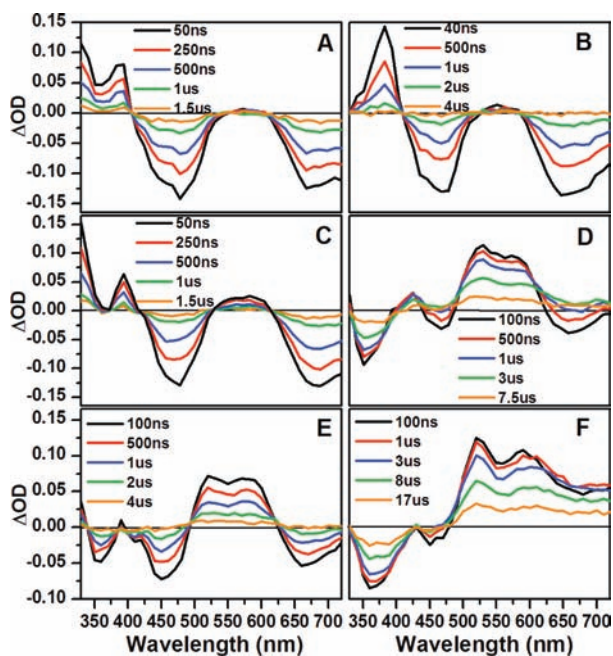
oxygen quenching measurements for the pyrene containing complexes. Lifetimes obtained by luminescence and transient absorption decays are summarized in Table 1.

Nanosecond Transient Absorption. Nanosecond time-resolved transient difference spectra provide a wealth of information about the nature of the excited states of the complexes. Samples were excited with output of a Nd:YAG pumped OPO at 460 nm and point by point transient spectra ($\Delta\text{abs. vs } \lambda$) were obtained every 10 nm between 330 and 700 nm. Spectra were generated from the collected decays at various times following excitation. Representative transient spectra of the three complexes are shown in Figure 5 for samples at pH 0 and 8. Figure 5, panels A and B, shows nanosecond transient behavior for $[\text{Ru}(\text{dcbH}_2)_2(\text{bpy})]^{2+}$, the parent complex, at the two pH values. The spectra both show a positive absorption in the 350–400 nm region and a bleach between 400 and 500 nm. The additional longer wavelength bleach signal in both spectra (>600 nm) results from luminescence of the complexes that is not corrected for in the experiment. Figure 5, panels C and D, illustrates the TA of the pyr-phen-bpy complex in acid and base. There are strong similarities between the parent complex and the pyr-phen-bpy complex spectra at pH 0. In base, the spectrum of the pyr-phen-bpy exhibits a bleach of the ground state absorption in the 400–500 nm region, but it is greatly diminished. A new bleach is observed between 300 and 400 nm and a broad positive absorption is evident from 500 to 600 nm. Thus there are obvious differences between the parent and the observed transient of the pyr-phen-bpy complex. Figure 5E shows the transient spectrum of the pyr-bpy complex in acid; the features are similar to the pyr-ph-bpy complex in base. In basic solution (Figure 5F), the transient absorption spectrum of the pyr-bpy complex is unique. It has a broad, positive transient absorption from 500 to 700 nm and bleaching between 360 and 460 nm.

In all cases the lifetimes of the TA signals obtained are comparable to those observed in luminescence. A key aspect of the transient difference decays is that they are cleanly single exponential in all cases; this contrasts the luminescence behavior of the pyr-bpy complex in basic solutions where a double exponential decay is observed. Since transient absorption spectra will reflect the relative concentrations of different species in solution whereas luminescence intensities

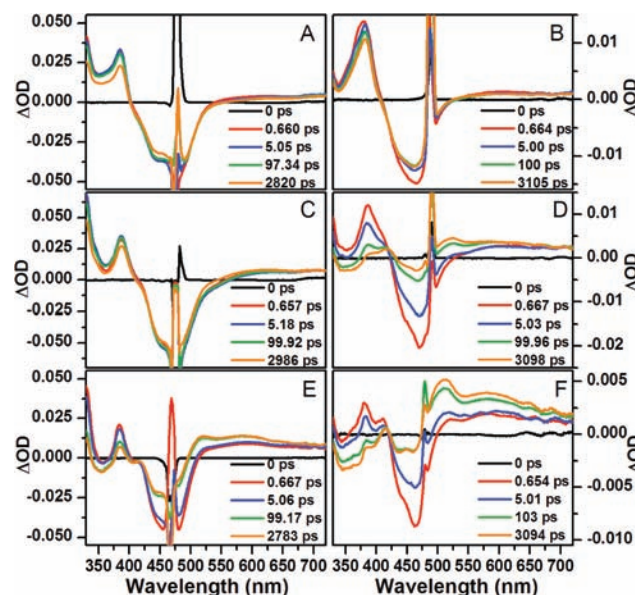
Table 1. Luminescence and Transient Absorption Decay Lifetimes of Complexes in Room Temperature Aqueous Methanol Solutions under Acidic and Basic Conditions

complex	bpy		pyr-bpy		pyr-ph-bpy	
	pH 0	pH 8	pH 0	pH 8	pH 0	pH 8
τ_{em} , μ s (λ_{obs} , nm)	0.611 ± 0.001 (668 nm)	0.926 ± 0.001 (636 nm)	1.87 ± 0.03 (664 nm)	17.7 ± 0.1 (637 nm)	1.19 ± 0.03 (665 nm)	4.65 ± 0.01 (636 nm)
τ_{TA} , μ s (λ_{obs} , nm)	0.61 ± 0.01 (390 nm)	0.94 ± 0.01 (450 nm)	1.8 ± 0.1 (360 nm)	15 ± 1 (360 nm)	0.70 ± 0.01 (390 nm)	5.6 ± 0.1 (350 nm)
τ_{TA} , μ s (λ_{obs} , nm)	0.70 ± 0.02 (660 nm)	1.1 ± 0.1 (630 nm)	1.7 ± 0.1 (520 nm)	15 ± 1 (520 nm)	0.91 ± 0.01 (660 nm)	5.3 ± 0.1 (520 nm)

**Figure 5.** Nanosecond transient absorption spectra for each of the chromophores at pH 0 (A, C, and E) and pH 8 (B, D, and F). (A) $[(dcbH_2)_2Ru(bpy)]^{2+}$, (B) $[(dcb)_2Ru(bpy)]^{2+}$, (C) $[(dcbH_2)_2Ru(pyr-ph-bpy)]^{2+}$, (D) $[(dcb)_2Ru(pyr-ph-bpy)]^{2+}$, (E) $[(dcbH_2)_2Ru(pyr-bpy)]^{2+}$, and (F) $[(dcb)_2Ru(pyr-bpy)]^{2+}$.

are a function not only of concentration but also emission efficiency, the short-lived component of the luminescence decays observed are believed to be associated with trace impurity emission (vide infra).

Ultrafast Transient Absorption. Since excitation of these complexes with visible light leads to generation of a singlet MLCT state that evolves into the thermally equilibrated state(s), reference tracking the evolution of these states from inception is certainly desirable. Collected spectra between <1 ps and 3 ns are shown in Figure 6 for the three complexes in acidic and basic solutions following 470 nm excitation with a 100 fs pulse. For $[Ru(dcbH_2)_2(bpy)]^{2+}$ the observed transient spectra in acidic and basic solution (Figure 6, panels A and B) include absorption between 350 and 400 nm as well as bleaching between 400 and 500 nm. The spectral features in the long time spectrum (~ 3000 ps) are similar to those that appear in the 50 ns spectra (excluding the emission observed in the ns spectra), with little evidence of dynamics in the earlier time spectra. The pyr-ph-bpy complex at pH 0 (Figure 6C) also has spectral features in the 3000 ps spectrum closely resembling the 50 ns spectrum. However, at pH 8 (Figure 6D), the initial spectrum acquired 660 (± 10) fs following excitation has well-defined absorption in the 300–400 nm region and bleaching

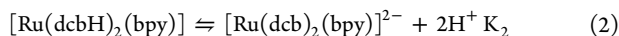
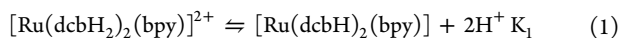
**Figure 6.** Subpicosecond transient absorption spectra for each of the chromophores at pH 0 (A, C, and E) and pH 8 (B, D, and F). (A) $[(dcbH_2)_2Ru(bpy)]^{2+}$, (B) $[(dcb)_2Ru(bpy)]^{2+}$, (C) $[(dcbH_2)_2Ru(pyr-ph-bpy)]^{2+}$, (D) $[(dcb)_2Ru(pyr-ph-bpy)]^{2+}$, (E) $[(dcbH_2)_2Ru(pyr-bpy)]^{2+}$, and (F) $[(dcb)_2Ru(pyr-bpy)]^{2+}$.

only between 400 and 500 nm; this sharply contrasts the spectrum obtained 100 ns after excitation (vide supra). During the time period from 660 fs to 3 ns the spectrum evolves such that the sharp absorption at 380 nm decays, concomitant with loss of the bleach at 460 nm. In addition, a clear isosbestic point is observed at 410 nm, suggesting clean evolution from the initially formed state to another state. Overall, the 3000 ps transient spectrum closely resembles the 100 ns transient spectrum. For the pyr-bpy complex (Figure 6, panels E and F), absorption at 660 fs after excitation also contains positive absorption between 350 and 400 nm as well as bleaching between 400 and 500 nm. Following this, changes occur that lead to bleaching between 350 and 380 nm, decreased MLCT bleaching and increased absorption between 500 and 700 nm. A similar, but more pronounced evolution of the spectral features is observed for this complex in pH 8 solution (Figure 6F), resulting in a spectrum after 3 ns that resembles the 100 ns spectrum, with significant bleaching between 300 and 400 nm and strong absorption to the red of 500 nm.

DISCUSSION

pH Dependence of MLCT Emission. The 3MLCT excited state of $[Ru(dcbH_2)_2(bpy)]^{2+}$ has two pK_a values, each corresponding to the loss of two protons. According to Nazeruddin et al.,²³ at sufficiently low pH, the molecule is fully

protonated and the $\text{Ru}(d\pi) \rightarrow \text{dcbH}_2(\pi^*)$ $^3\text{MLCT}$ state is the lowest energy state. The energy of the MLCT transition to the dcbH_n ligand is raised as the ligand is deprotonated. When the carboxybipyridine is fully deprotonated, the $\text{Ru}(d\pi) \rightarrow \text{dcb}(\pi^*)$ $^3\text{MLCT}$ state energy has been raised to the point where the state is higher in energy than the $\text{Ru}(d\pi) \rightarrow \text{bpy}(\pi^*)$ $^3\text{MLCT}$ transition. Based on the work of Nazeruddin and co-workers,²³ the two $\text{p}K_a$ values measured for $[\text{Ru}(\text{dcbH}_2)_2(\text{bpy})]^{2+}$ are 1.8 and 4.5 and can be represented as sequential deprotonation of both of the carboxylated bipyridine ligands as shown in eqs 1 and 2 below.



As stated earlier, the implication is that electronic interaction of the two coordinated carboxybipyridine ligands is sufficiently weak that acid dissociation of a carboxylic acid on one ligand does not influence the similar dissociation on the other carboxy bipyridyl ligand. As a result, the double deprotonations of eqs 1 and 2 can be treated as two nearly identical and independent equilibria. Similar behavior is observed for the pyr-bpy and pyr-ph-bpy complexes in aqueous methanol solutions buffered between pH 0 and 8. Figure 7 shows the dependence of the

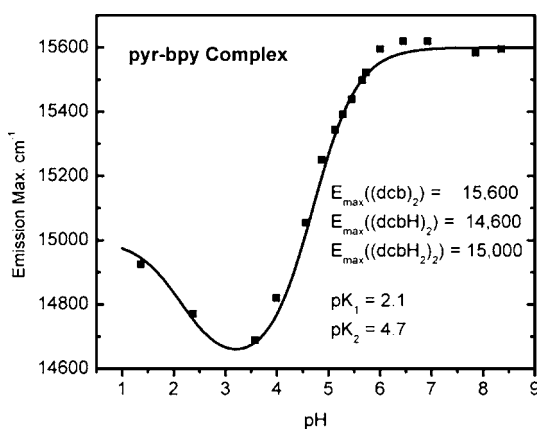


Figure 7. Emission maxima of $[(\text{dcbH}_n)_2\text{Ru}(\text{pyr-bpy})]^{(2+2n)}$ ($n = 0-2$) in 1:1 methanol:water as a function of pH. The solid line represents a fit to eq 3 using the parameters shown in the figure.

emission maximum on pH for $[(\text{dcbH}_n)_2\text{Ru}(\text{pyr-bpy})]^{(2+2n)}$ ($n = 0-2$). The spectral bandwidth remains relatively constant over the entire pH range, suggesting that the emission spectra reflect the average equilibrated degree of protonation of the complexes. The collected emission maxima can then be modeled assuming the maximum at any given pH represents the weighted average of the $[\text{Ru}(\text{dcbH}_2)_2(\text{pyr-bpy})]^{2+}$ (H_2A), $[\text{Ru}(\text{dcbH})_2(\text{pyr-bpy})]$ (HA), and $[\text{Ru}(\text{dcb})_2(\text{pyr-bpy})]^{2-}$ (A) forms of the complex as given by eq 3. The fractions, f_i , of each of the forms of the acid at any given pH were determined from the K_1 and K_2 values for the

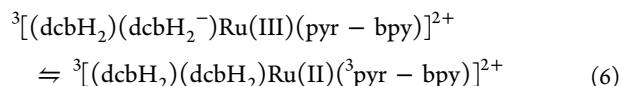
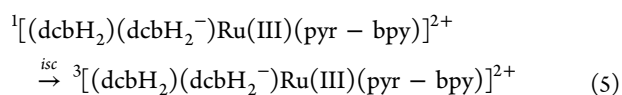
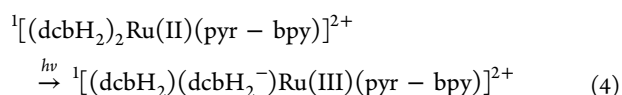
$$E^{\text{CT}} = f_{\text{H}_2\text{A}} E_{\text{H}_2\text{A}} + f_{\text{HA}} E_{\text{HA}} + f_{\text{A}} E_{\text{A}} \quad (3)$$

two acid dissociations of eqs 1 and 2 and the emission maxima of each of the three forms of the complex were fitting parameters. Results are shown for the pyr-bpy complex in Figure 7 (solid line and parameters of fit); the two $\text{p}K$ values, 2.1 and 4.7, are slightly higher than those determined by Nazeruddin et al. for $[\text{Ru}(\text{dcbH}_2)_2(\text{bpy})]^{2+23}$ but are in

generally good agreement given the similarity of the complexes. The calculated maxima provide approximate values of the emission energy for each form of the complex; these can be used in evaluation of the relative energies of the MLCT and pyrene localized triplet states (vide infra). An interesting observation is that the emission maximum of the partially deprotonated complex is lower in energy than the fully protonated complex. This reflects the fact that the initial deprotonation steps will have a significant contributing portion of a monodeprotonated complex, $[(\text{dcbH}_2)(\text{dcbH})\text{Ru}(\text{bpy})]^{+}$; the monodeprotonated ligand should be a somewhat better σ donor than the fully protonated species and will serve to raise the energy of the $d\pi$ orbitals of the Ru, thereby slightly lowering ($\sim 400 \text{ cm}^{-1}$) the energy of the emission of the remaining $\text{Ru}(d\pi) \rightarrow \text{dcbH}_2(\pi^*)$ MLCT state. This fourth form of the complex was not used in fitting the pH dependence of the luminescence since good fits were obtained with only the three (H_2A , HA , and A).

pH Dependence of Transient Spectra. When the complexes are excited at wavelengths to the red of 430 nm, the initial state populated is the $^1\text{MLCT}$ state. This state evolves into the thermally equilibrated excited state(s) of the complex from which luminescence or, in this case, reaction with oxygen may occur. At issue is the nature of the lowest excited state. One possibility is complete localization as a $\text{Ru}(d\pi) \rightarrow \text{dcbH}_2(\pi^*)$ $^3\text{MLCT}$, $\text{Ru}(d\pi) \rightarrow \text{dcb}(\pi^*)$ $^3\text{MLCT}$, $\text{Ru}(d\pi) \rightarrow \text{bpy}(\pi^*)$ (or pyr containing $\text{bpy}(\pi^*)$) $^3\text{MLCT}$ or $\text{pyr} \pi \rightarrow \pi^*$ ^3IL state. Alternatively the thermally equilibrated state could be a single excited state with contributions from two or more of these states, or an equilibrium mixture of two or more of the states. The transient spectra shown in Figures 5 and 6 clearly illustrate that there are significant differences in the spectra of the pyrene containing complexes in acidic and basic solution. The ns and fs transient spectra of $[\text{Ru}(\text{bpy})_3]^{2+}$ have been thoroughly investigated.²⁹⁻³² The ns spectrum is characterized by an absorption at 360 nm attributed to absorption of the bpy anion radical of the $^3\text{MLCT}$ state. This is accompanied by bleaching of the ground state absorbance centered at 454 nm.³³ In the fs spectrum of $[\text{Ru}(\text{bpy})_3]^{2+}$ the features characteristic of the thermally equilibrated $^3\text{MLCT}$ state are evident 300 fs following excitation.¹⁵ The $[(\text{dcbH}_n)_2\text{Ru}(\text{bpy})]^{(2+2n)}$ ($n = 0-2$) series clearly shows the spectral features that can be readily associated with $[\text{Ru}(\text{bpy})_3]^{2+}$, in both acidic and basic solutions. In this work, the spectral features appear within less than a ps after excitation for the bpy complex in acidic and basic solution and persist throughout the excited state decay. The absorption feature between 300 and 400 nm differs between acidic solutions, where the $\text{Ru}(d\pi) \rightarrow \text{dcbH}_2(\pi^*)$ $^3\text{MLCT}$ state is the lowest energy state and solutions above pH 7, where either the $\text{Ru}(d\pi) \rightarrow \text{bpy}(\pi^*)$ or the $\text{Ru}(d\pi) \rightarrow \text{dcb}(\pi^*)$ $^3\text{MLCT}$ state is populated.

Previous investigations of Ru(II) complexes of pyr-bpy and related complexes illustrate significant differences in the ns transient absorption behavior.^{5,10,18,20,34} The key difference relative to $[\text{Ru}(\text{bpy})_3]^{2+}$ is the appearance of strong transient absorption between 500 and 800 nm. The kinetic behavior of the two pyrene containing complexes clearly shows evolution of the initially formed excited state, an MLCT state by virtue of the excitation wavelength, to what we are presuming to be an equilibrium mixture of a $^3\text{MLCT}$ state with the ^3IL state localized on the pyrene containing ligand. The sequence of events is shown below in eqs 4-6 for the pyr-bpy complex in acidic solution.



Excitation to the ${}^1\text{MLCT}$ state is followed by intersystem crossing to the ${}^3\text{MLCT}$ state, determined to be <1 ps for a variety of Ru(II) diimine complexes closely related to the systems studied here.^{15,32} Energy transfer from the ${}^3\text{MLCT}$ state to the ${}^3\text{IL}$ state, k_{en} , and back energy transfer, $k_{-\text{en}}$ will occur and equilibrium can be established. Rate constants for energy transfer from the ${}^3\text{MLCT}$ to ${}^3\text{IL}$ state are given in Table 2. The results are obtained from the temporal evolution of

Table 2. Kinetic Parameters Obtained from Fits of ps and ns Time Resolved Decays and Estimated Energy of the ${}^3\text{IL}$ State

	pyr-bpy		pyr-ph-bpy	
	pH 0	pH 8	pH 0	pH 8
$k_{\text{CT}}(\text{MLCT}) \text{ s}^{-1}$	1.5×10^6	1.0×10^6	1.5×10^6	1.0×10^6
$k_{\text{IL}}(\text{IL}), \text{ s}^{-1}$	1.0×10^4	1.0×10^4	1.0×10^4	1.0×10^4
$k_{\text{en}}, \text{ s}^{-1}$	1.6×10^{10}	3.6×10^{10}	4.0×10^9	1.6×10^{10}
K_{EQ}	1.6	16	0.10	4.4
$k_{-\text{en}}, \text{ s}^{-1}$	1.0×10^{10}	2.3×10^9	4.0×10^{10}	3.6×10^9
$\Delta G, \text{ cm}^{-1}$	-90	-570	480	-310
$E_{\text{IL}}, \text{ cm}^{-1}$	14900	15200	15400	15400

transient spectra on the ps/ns time scale as shown in Figure 6 for all of the complexes in acidic and basic solution. In each case the energy gap between the ${}^3\text{MLCT}$ and ${}^3\text{IL}$ states is small ($<1000 \text{ cm}^{-1}$; $<0.125 \text{ eV}$) and, as a result, the reverse energy transfer process ($k_{-\text{en}}$, Figure 1) should be on the ns or subns time scale. Since the shortest lived excited state of the pyrene

containing complexes in any aqueous methanol solution is at least 500 ns and the forward and reverse energy transfer processes are fast relative to this rate of decay, it is safe to assume that the excited states are indeed in equilibrium during relaxation to the ground state.

For the pyr-ph-bpy complex the reaction sequence follows that of eqs 4–6 and Figure 1. In acidic solution the ultrafast transient absorption indicates formation of the ${}^3\text{MLCT}$ state in <1 ps. The spectrum of this state matches that of the complex on the ns to μs time scale. There is, however, a small absorption signal to the red of 500 nm that grows in over the first 1000 ps; the rate constant for this process is determined is $4 \times 10^9 \text{ s}^{-1}$ (250 ps, Table 2) from fits of the transient rise at 590 nm as well as the decay of the bleach at 450 nm. We have attributed this process to equilibration of the ${}^3\text{MLCT}$ state with the pyr-ph-bpy localized ${}^3\text{IL}$ state via energy transfer. In this case, the transient spectrum obtained on the ns time scale indicates that the position of equilibrium of the excited state is largely localized on the ${}^3\text{MLCT}$ state, as evidenced by the transient absorption between 350 and 400 nm as well as a small absorption at wavelengths longer than 500 nm.

In basic solution, the transient spectrum of the pyr-ph-bpy complex exhibits significant changes in band shape in the first 1000 ps (Figure 6D). The features of the initially formed ${}^3\text{MLCT}$ state disappear and are accompanied by the appearance of the ${}^3\text{IL}$ spectrum. The rate constant for this process, $2 \times 10^{10} \text{ s}^{-1}$, is a factor of 5 faster than the corresponding process in acidic solution. The 100 ns transient spectrum (Figure 5D) has the features of the pyrene ${}^3\text{IL}$ spectrum, but also includes emission of the ${}^3\text{MLCT}$ state. Nonetheless, it is clear that, qualitatively, the equilibrium favors the ${}^3\text{IL}$ state at pH 8, consistent with the raising of the ${}^3\text{MLCT}$ state following deprotonation.

In both acidic and basic solution the transient spectrum of the pyr-bpy complex clearly evolves from the ${}^3\text{MLCT}$ to the ${}^3\text{IL}$ spectrum over the first ns. Rate constants for the process are $2 \times 10^{10} \text{ s}^{-1}$ (50 ps) at pH 0 and $4 \times 10^{10} \text{ s}^{-1}$ (25 ps) at pH 8. Spectra on the μs time scale in acidic solution include features of both states, with bleaching of the MLCT absorption (450 nm) and strong ${}^3\text{IL}$ absorption to the red of 500 nm. At pH 8

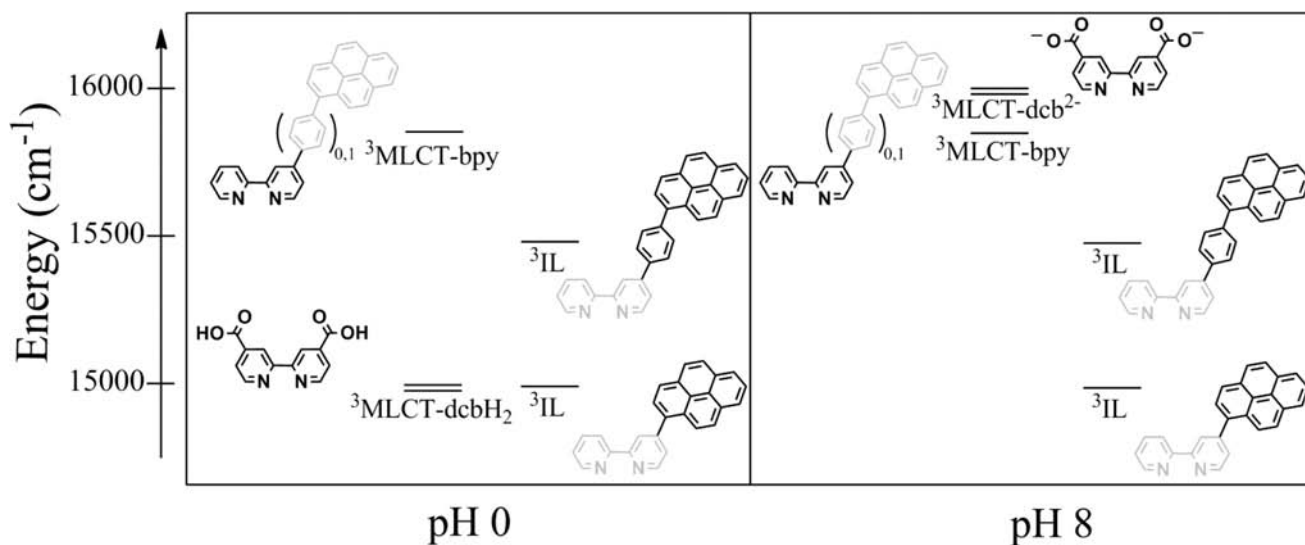


Figure 8. Relative energy diagram for compounds containing coupled ${}^3\text{MLCT}$ and aromatic hydrocarbon ${}^3\text{IL}$ (${}^3\pi-\pi^*$) states. The relative energies are shown together for both the pyr-bpy and the pyr-ph-bpy complexes.

the transient absorption spectrum lacks any features of the $^3\text{MLCT}$ state (Figures 5F and 6F).

The key observation for the pyrene containing complexes is that the position of equilibrium changes from an excited state nearly completely localized on the $^3\text{MLCT}$ ($\text{Ru}(\text{d}\pi) \rightarrow \text{dcbH}_2(\pi^*)$) state to a ^3IL ($^3\text{pyr}(\pi \rightarrow \pi^*)$) state simply by variation of the solution pH from 3 to 8. The relative energies of the states, obtained from analysis of the excited state decays (vide infra), are shown in Figure 8 for the two complexes.

Excited State Equilibria and Decay. Since the excited states of the pyrene containing complexes can be assumed to be in equilibrium, relaxation to the ground state will occur with a rate constant that is the weighted average of the decay rate constants of the $^3\text{MLCT}$, k_{CT} , and the ^3IL , k_{IL} , states (eq 7).³⁵

$$k_{\text{obs}} = f_{\text{CT}}(k_{\text{CT}}) + f_{\text{IL}}(k_{\text{IL}}) \quad (7)$$

The excited state lifetime of the $^3\text{MLCT}$ state is pH dependent and can be approximated from the lifetime of the parent complex, $[(\text{dcbH}_n)_2\text{Ru}(\text{bpy})]^{(2n-2)}$ ($n = 0-2$); values used for k_{CT} are given in Table 2. On the other hand, no suitable simple model exists for estimation of k_{IL} for either of the pyrene containing ligands. However, the collected transient spectral results indicate that, in acidic solution, the MLCT state is the major state populated (vide supra), providing a lower boundary on the energy of the ^3IL state (in acid $E_{\text{MLCT}} < E_{\text{pyr}}$). In basic solution, the ^3IL state is the predominant state observed, and here the energy of the observed emission can be used as an upper limit on the pyrene triplet state energy. Collectively, the observations bound the free energy for the intramolecular energy transfer (eq 6) to be well below 1000 cm^{-1} , thereby limiting the equilibrium constant at any given pH to be between 0.01 (in acid) and 100 (in base). With these boundaries and the observed excited state decays, it is clear that once the decay rate constant of the ^3IL state is slower than 10^4 s^{-1} (much faster than that for triplet pyrene, for example),³⁶ the observed decay rate constant will be completely dominated by the fraction of the $^3\text{MLCT}$ state. With this restriction, a decay rate constant of 10^4 s^{-1} was used for the ^3IL state of both pyrene containing complexes. The observed rate constant, k_{obs} , can be expressed in terms of K_{eq} for the equilibrium expressed in eq 6. This expression for k_{obs} was included in the exponential decay function and used to fit nanosecond absorption decays (eq 8).

$$\Delta(\text{Abs})_t = \Delta(\text{Abs})_0 \exp \left[\left(\left(1 - \frac{K_{\text{eq}}}{K_{\text{eq}} + 1} \right) k_{\text{CT}} + \left(\frac{K_{\text{eq}}}{K_{\text{eq}} + 1} \right) k_{\text{IL}} \right) t \right] + b \quad (8)$$

The assumed values for the rate constants, k_{CT} and k_{IL} , are justified above and shown in Table 2. K_{eq} is the only variable and b is a baseline residual that is nearly zero in all cases. The forward energy transfer rate constants are available from the ultrafast transient data; therefore, back energy transfer rate constants can also be obtained once a value for K_{eq} is determined.

The free energies for the energy transfer processes for both the pyr-bpy and the pyr-ph-bpy complexes at pH 0 and pH 8 are determined directly from the equilibrium constants obtained from fits of the transient absorption decays. Given these and the energies of the $^3\text{MLCT}$ state at each pH (from

the emission spectra of the bpy complex), the energy of the ^3IL state can be approximated. The collected values are given in Table 2. For the pyr-bpy complex, the energy of the ^3IL state obtained in this way differs by 300 cm^{-1} between values obtained in acid and base and the average is approximately $15\,000 \text{ cm}^{-1}$. For the pyr-ph-bpy complex the ^3IL energy is $15\,400 \text{ cm}^{-1}$ in both determinations.

The results for the two chromophores are summarized by Figure 8 which presents, semiquantitatively, the energy differences between the various states involved at different degrees of protonation. It is assumed that the energy of the ^3IL state is unaffected by pH. In acidic solution, the $\text{Ru}(\text{d}\pi) \rightarrow \text{dcbH}_2(\pi^*)$ $^3\text{MLCT}$ state is lowest in energy for the pyr-ph-bpy complex, but the ^3IL and $^3\text{MLCT}$ (dcbH_2) are nearly isoenergetic for the pyr-bpy complex. Upon raising the pH above pH 7, the thermally equilibrated lowest energy $^3\text{MLCT}$ state, either $\text{Ru}(\text{d}\pi) \rightarrow \text{dcb}(\pi^*)$ or $\text{Ru}(\text{d}\pi) \rightarrow \text{bpy}(\pi^*)$, lies above the ^3IL state by approximately 300 cm^{-1} for the pyr-ph-bpy complex and 600 cm^{-1} for the pyr-bpy complex.

These results were borne out clearly in the ns transient absorption spectra (Figure 5). In acidic solution, the pyr-bpy complex shows features of the ^3IL state, whereas the pyr-ph-bpy complex appears to be dominated by the $^3\text{MLCT}$ state. In base, both complexes exhibit spectral features of the ^3IL excited state.

Oxygen Quenching. Both the luminescence intensity and lifetime of all the complexes are quenched by dissolved oxygen in aqueous methanol. Figure 4 illustrates the pH dependence of the degree of quenching of the emission lifetime as a function of dissolved oxygen from aerated solutions for both of the pyrene containing complexes. The quenching ratio for $[\text{Ru}(\text{dcbH}_n)_2(\text{bpy})]^{(2n-2)}$ ($n = 0-2$) is only weakly pH dependent and is around 2 for acidic and basic solutions. Rate constants for oxygen quenching of the three complexes in neutral aqueous methanol (pH 7) solutions ($[\text{O}_2] \approx 6 \times 10^{-4} \text{ M}$),³⁷ measured from luminescence lifetime changes between oxygen free and air saturated solutions, are the same for all of the complexes ($2 \pm 1 \times 10^9 \text{ M}^{-1}\text{s}^{-1}$). Thus, the large differences in the magnitude of the quenching shown in Figure 4 are the result of differences in the excited state lifetimes of the complexes. The pH dependence for quenching of the two pyrene containing complexes can also be evaluated in relation to the fractional equilibrium occupation of the pyrene localized triplet state. Using the two acid dissociation constants (eqs 1 and 2, $\text{p}K_1 = 2.1$ and $\text{p}K_2 = 4.7$), the oxygen concentration in the mixed methanol:water solution and the lifetimes of the respective complexes at pH 0 and pH 8, the lifetime quenching curve can be as given as a modified Stern–Volmer equation (eq 9). The terms k_{acid} , k_{inter} , and k_{base} are the inverse excited state lifetimes at

$$\frac{\tau_0}{\tau} = 1 + (f_{\text{acid}} k_{\text{acid}} \tau_{\text{acid}} + f_{\text{inter}} k_{\text{inter}} \tau_{\text{inter}} + f_{\text{base}} k_{\text{base}} \tau_{\text{base}}) [\text{O}_2] \quad (9)$$

pH 0, an intermediate pH and pH 8, respectively. In fits to eq 9 the rate constant for quenching of the acidic and intermediate forms of the complex is assumed to be the same (quenching of the $^3\text{MLCT}$ state differs from that of the ^3IL state). Fits yield rate constants of 5×10^8 and $2 \times 10^9 \text{ M}^{-1} \text{ s}^{-1}$ for quenching of the acidic/intermediate and basic forms, respectively (Figure 4). Poor fits are obtained by using only a single quenching rate constant k_{q} for all three forms of the complex, also shown in figure 4 for the pyr-bpy complex; clearly a single quenching rate constant is not adequate to describe the behavior of this system.

This is not surprising given the very different nature of the two excited states in equilibrium.

The implication of these results is that the overall efficacy of oxygen sensors derived from Ru(II) diimine complexes covalently linked to pyrene (or other aromatic hydrocarbons with triplet energies close to that of the Ru(II) complex $^3\text{MLCT}$ state) is dependent principally on the position of the equilibrium between the $^3\text{MLCT}$ state and the ^3IL state and the excited state lifetime of the ^3IL state. As long as luminescence can be observed from the complex, the limiting lifetime of the excited complex will increase with an increase in the fraction of the ^3IL state (eq 6) and a decrease in the excited state decay rate constant of the aromatic hydrocarbon. Given these restrictions, the pyr-bpy complex in basic solution provides very nearly the limiting case oxygen sensing ability and is limited by the decay rate constant of the pyrene triplet.

SUMMARY

The photophysical behavior of two Ru(II) complexes having a covalently linked, nonabsorbing pyrene partner for electronic energy transfer were examined. Each complex has carboxy-bipyridine ligands that allow control of the energy of the emissive $^3\text{MLCT}$ state of the complex over the pH range 0–8, thereby allowing variation of the energy gap between the $^3\text{MLCT}$ state and the pyrene localized ^3IL state. The key observation of the work is that energy transfer between the $^3\text{MLCT}$ and ^3IL states can be controlled by varying the pH of the system. From analysis of the pH dependence of the emission energy of a model complex, acid dissociation constants for the carboxylate substituents on the bipyridine ligands could be extracted. Further analysis of the luminescence decays of the pyrene complexes and the transient absorption features provided clear evidence that the two excited states are in equilibrium and that relaxation to the ground state is a weighted average of the decays of the $^3\text{MLCT}$ and ^3IL states. Detailed analysis of pH 0 and 8 excited state decays allowed determination of the energy gap between the two states as well as the energy of the spectroscopically silent ^3IL state. Oxygen quenching of the complexes occurred with a rate constant of $2 \pm 1 \times 10^9 \text{ M}^{-1} \text{ s}^{-1}$ in mixed water/methanol. The degree of oxygen quenching observed varies over a wide range with changes in pH and reflects the change in the position of the equilibrium between the $^3\text{MLCT}$ and ^3IL states. Higher fractional occupation of the ^3IL state results in a longer excited state lifetime in the absence of oxygen and a higher degree of oxygen quenching. The results are useful in guiding the design of phosphorescent sensors for in vivo oxygen sensing in hypoxic environments, where the need to maximize oxygen quenching efficiency is paramount.

AUTHOR INFORMATION

Corresponding Author

russ@tulane.edu

Notes

The authors declare no competing financial interest.

ACKNOWLEDGMENTS

R.H.S. thanks the U.S. Department of Energy, Office of Chemical Sciences (Grant DE-FG-02-96ER14617) for supporting this research and the National Science Foundation (Grant CHE0619770) for funding the ESI mass spectrometer. T.G. thanks the Louisiana Board of Regents for a BOR Graduate

Fellowship. J.J.R. acknowledges the National Science Foundation for funding of this project (CHE 0809699, CHE 0947031, and CHE 1112250).

REFERENCES

- (1) Subotnik, J. E.; Vura-Weis, J.; Sodt, A. J.; Ratner, M. A. *J. Phys. Chem. A* **2010**, *114*, 8665–8675.
- (2) Vagnino, M. T.; Caleb Rutledge, W.; Wagenknecht, P. S. *Inorg. Chem.* **2010**, *49*, 833–838.
- (3) Merkel, P. B.; Dinnocenzo, J. P. *J. Photochem. Photobiol. A* **2008**, *193*, 110–121.
- (4) Demas, J. N. In *Excited state lifetime measurements*; Academic Press: New York, 1983; pp 273.
- (5) Simon, J. A.; Curry, S. L.; Schmehl, R. H.; Schatz, T. R.; Piotrowiak, P.; Jin, X.; Thummel, R. P. *J. Am. Chem. Soc.* **1997**, *119*, 11012–11022.
- (6) Harriman, A.; Hissler, M.; Khatyr, A.; Ziesel, R. *Chem. Commun. (Cambridge)* **1999**, 735–736.
- (7) Sohna Sohna, J.; Carrier, V.; Fages, F.; Amouyal, E. *Inorg. Chem.* **2001**, *40*, 6061–6063.
- (8) Gu, J.; Chen, J.; Schmehl, R. H. *J. Am. Chem. Soc.* **2010**, *132*, 7338–7346.
- (9) Tyson, D. S.; Henbest, K. B.; Bialecki, J.; Castellano, F. N. *J. Phys. Chem. A* **2001**, *105*, 8154–8161.
- (10) Del Guerso, A.; Leroy, S.; Fages, F.; Schmehl, R. H. *Inorg. Chem.* **2002**, *41*, 359–366.
- (11) Benniston, A. C.; Harriman, A.; Lawrie, D. J.; Mayeux, A. *Phys. Chem. Chem. Phys.* **2004**, *6*, 51–57.
- (12) Wang, X. Y.; DelGuerso, A.; Schmehl, R. H. *J. Photochem. Photobiol., C* **2004**, *5*, 55–77.
- (13) Balazs, G. C.; del Guerso, A.; Schmehl, R. H. *Photochem. Photobiol. Sci.* **2005**, *4*, 89–94.
- (14) Ji, S.; Wu, W.; Guo, H.; Zhao, J. *Angew. Chem., Int. Ed.* **2011**, *50*, 1626–1629.
- (15) Yeh, A. T.; Shank, C. V.; McCusker, J. K. *Science* **2000**, *289*, 935–938.
- (16) Wallin, S.; Davidsson, J.; Modin, J.; Hammarström, L. *J. Phys. Chem. A* **2005**, *109*, 4697–4704.
- (17) Henry, W.; Coates, C. G.; Brady, C.; Ronayne, K. L.; Matousek, P.; Towrie, M.; Botchway, S. W.; Parker, A. W.; Vos, J. G.; Browne, W. R.; McGarvey, J. J. *J. Phys. Chem. A* **2008**, *112*, 4537–4544.
- (18) Schmehl, R. *Spectrum (Bowling Green, OH, U. S.)* **2000**, *13*, 17–21.
- (19) Tyson, D. S.; Castellano, F. N. *Abstracts of Papers*, 220th ACS National Meeting, Washington, DC, United States, August 20–24, 2000; INOR-237.
- (20) Tyson, D. S.; Castellano, F. N. *J. Phys. Chem. A* **1999**, *103*, 10955–10960.
- (21) Choi, N.; Stroock, A.; Verbridge, S.; Williams, R.; Kim, J.; Chen, J.; Schmehl, R. H.; Zipfel, W. R.; Farnum, C. E. *Biomaterials* **2012**, *33*, ASAP.
- (22) Giordano, P. J.; Bock, C. R.; Wrighton, M. S.; Interrante, L. V.; Williams, R. F. X. *J. Am. Chem. Soc.* **1977**, *99*, 3187–9.
- (23) Nazeeruddin, M. K.; Kalyanasundaram, K. *Inorg. Chem.* **1989**, *28*, 4251–4259.
- (24) Cordaro, J. G.; McCusker, J. K.; Bergman, R. G. *Chem. Commun.* **2002**, 1496–1497.
- (25) Hoertz, P. G.; Staniszewski, A.; Marton, A.; Higgins, G. T.; Incarvito, C. D.; Rheingold, A. L.; Meyer, G. J. *J. Am. Chem. Soc.* **2006**, *128*, 8234.
- (26) Nazeeruddin, M. K.; Zakeeruddin, S. M.; Humphrey-Baker, R.; Jirousek, M.; Liska, P.; Vlachopoulos, N.; Shklover, V.; Fischer, C. H.; Graetzel, M. *Inorg. Chem.* **1999**, *38*, 6298–6302.
- (27) Freedman, D. A.; Evju, J. K.; Pomije, M. K.; Mann, K. R. *Inorg. Chem.* **2001**, *40*, 5711–5714.
- (28) Chen, J. *Ruthenium(II) Pyrene-Bipyridine Complexes: Synthesis, Photophysics, Photochemistry and in Vivo Oxygen Sensing*; Tulane University: New Orleans, LA, 2010.

- (29) Curtright, A. E.; McCusker, J. K. *J. Phys. Chem. A* **1999**, *103*, 7032–7041.
- (30) Damrauer, N. H.; Boussie, T. R.; Devenney, M.; McCusker, J. K. *J. Am. Chem. Soc.* **1997**, *119*, 8253–8268.
- (31) Damrauer, N. H.; Cerullo, G.; Yeh, A.; McCusker, J. K. *Springer Ser. Chem. Phys.* **1998**, *63*, 627–629.
- (32) Damrauer, N. H.; McCusker, J. K. *J. Phys. Chem. A* **1999**, *103*, 8440–8446.
- (33) Juris, A.; Balzani, V.; Barigelletti, F.; Campagna, S.; Belser, P.; Von Zelewsky, A. *Coord. Chem. Rev.* **1988**, *84*, 85–277.
- (34) Harriman, A.; Khatyr, A.; Ziessel, R. *Dalton Trans.* **2003**, 2061–2068.
- (35) Ford, W. E.; Rodgers, M. A. J. *J. Phys. Chem.* **1992**, *96*, 2917–20.
- (36) Birks, J. B. *J. Phys. Chem.* **1963**, *67*, 2199–2200.
- (37) Korall, P.; Boerje, A.; Norrby, P. O.; Aakermark, B. *Acta Chem. Scand.* **1997**, *51*, 760–766.